The Journal of Navigation (2022), **75**:1 57–75
doi:10.1017/S0373463321000795

RESEARCH ARTICLE

Maritime navigational assistance by visual augmentation

Bruno G. Leite,* Helio T. Sinohara, Newton Maruyama, and Eduardo A. Tannuri

Escola Politécnica, Universidade de São Paulo.
*Corresponding author. E-mail: bruno.giordano.leite@usp.br

Received: 10 June 2021; **Accepted:** 23 September 2021; **First published online:** 29 October 2021

Keywords: e-navigation; numerical simulation; display; graphic user interface (GUI)

Abstract

Several types of equipment have been developed over the years to assist ship operators with their tasks. Nowadays, navigational equipment typically provides an enormous volume of information. Thus, there is a corresponding need for efficiency in how such information is presented to ship operators. *Augmented reality* (AR) systems are being investigated for such efficient presentation of typical navigational information. The present work is particularly interested in an AR architecture commonly referred as *monitor augmented reality* (MAR).

In this context, the development of MAR systems is briefly summarised. The projection of three-dimensional elements into a camera scene is presented. Potential visual assets are proposed and exemplified with videos from a ship manoeuvring simulator and a real experiment. Enhanced scenes combining pertinent virtual elements are shown exemplifying potential assistance applications. The authors mean to contribute to the popularisation of MAR systems in maritime environments. Further research is suggested to define optimal combinations of visual elements for alternative maritime navigation scenarios. Note that there are still many challenges for the deployment of MAR tools in typical maritime operations.

1. Introduction

One of the most important challenges associated with enabling world-wide commercial navigation relates to safety. Institutions, regulations and procedures have been developed over time to ensure *safety at sea*, which have considered *'such desirable conditions of human activity at sea that do not endanger human life and property, and are not harmful to the maritime environment'* (Kopacz et al., 2001). Different scientific and technological advances have contributed to both economic feasibility and safety of maritime navigation. Particularly, fields such as electronics, radio, computer science, automatic control engineering, data presentation and space technologies have led to the development of integrated equipment and systems to assist in the ship's operation (Kopacz et al., 2004). Note that as the human activity at the sea increases, there is a corresponding need for general improvements in overall safety and efficiency of maritime operations. Further usability studies have been proposed towards the development of optimal user interfaces for maritime equipment (Hareide and Ostnes, 2017).

Technological trends, such as autonomous vehicles and robotics; artificial intelligence; big data; virtual, augmented and mixed reality; internet of things; cloud and edge computing; digital security; and three-dimensional printing and additive engineering, have recently been investigated towards improvements in the performance of existing maritime operations (Sanchez-Gonzalez et al., 2019). The incorporation of new navigation-related technologies in maritime equipment is usually associated with an increase in the amount of information and alerts displayed (Maglić and Zec, 2020).

Tools with augmented reality (AR) methods have been proposed for presenting navigational data. Such tools may facilitate the interpretation of navigational information during operation. Holder and

Pecota (2011) conducted tests with full-mission simulations for the definition of operational requirements for a maritime head-up display (HUD) system. Alternative types of AR solutions (monitor augmented reality; MAR) uses a monitor for displaying navigational information (Morgère et al., 2014; Hong et al., 2015; Oh et al., 2016; Mihoc and Cater, 2017). A systematic review regarding the use of augmented reality technology in the field of maritime navigation is presented by Laera et al. (2021).

Usability and precision considerations regarding the full development of an operational MAR system are beyond the scope of the present work. Instead, a preliminary investigation is proposed towards the development of a MAR system for navigational assistance in restricted waters. In such a system, a monitor displays the scene measured by a camera that is rigidly attached to the ship. Virtual elements are rendered on top of the navigation scene to assist with their perception.

In the following section, foundations for augmented reality systems are briefly summarised. Next, the synthesis of virtual elements in maritime scenes is proposed with navigation experiments. The experiments assume that the camera is rigidly attached to the ship in a MAR setup. Finally, potential navigational assistance applications are discussed with examples of augmented scenes that combine pertinent virtual elements.

2. Methods

2.1. Augmented reality

The beginnings of augmented reality technology can be dated back to a pioneer work in the 1960s. A see-through head-mounted device (HMD) was designed to present three-dimensional graphics (Sutherland, 1968). The fundamental idea behind the three-dimensional display proposed in the work was to present the user with a perspective image which changes as he moves. As the retinal images measured by eyes are two-dimensional projections, it is possible to create three-dimensional object illusions by placing suitable two-dimensional images on the observer's retina.

Two different coordinate systems have been defined: the *room coordinate system* and the *eye coordinate system*. The viewer position and orientation is estimated at all times with a tracking device. These estimates yields the instantaneous transformation from the room coordinate system to the eye coordinate system. Reference points are described in the *room* coordinate system. The coordinates of these points are transformed to the *eye* coordinate system and then projected into the image scene with perspective projection models.

Over the years that followed, further research on the proposed concept resulted in the emergence of augmented reality as a research field. Milgram et al. (1995) categorised augmented reality displays into two subclasses: *see-through* and *monitor-based* displays. See-through displays are inspired by the earlier work of Sutherland (1968), while monitor-based displays refer to those in which computer-generated images are overlaid onto live or stored video images. Furthermore, Azuma (1997) published an important survey summarising the main developments up to that point. Figure 1 shows a conceptual diagram for a monitor-based system.

Generally, a set of virtual points to be displayed is defined with respect to a coordinate system external to the camera. For each image measured by the camera, the corresponding transformation between the camera coordinate system and this external coordinate system is applied for the set of virtual points.

2.2. Camera projection

Consider a *world coordinate system* described with axes $[\vec{x}, \vec{y}, \vec{z}]$ and a *ship coordinate system* described with axes $[\vec{i}, \vec{j}, \vec{k}]$. Each axis from the world coordinate system may be expressed as a combination of axes from the ship coordinate system:

$$\vec{x} = x_i\vec{i} + x_j\vec{j} + x_k\vec{k}, \quad \vec{y} = y_i\vec{i} + y_j\vec{j} + y_k\vec{k}, \quad \vec{z} = z_i\vec{i} + z_j\vec{j} + z_k\vec{k} \tag{2.1}$$

https://doi.org/10.1017/S0373463321000795 Published online by Cambridge University Press

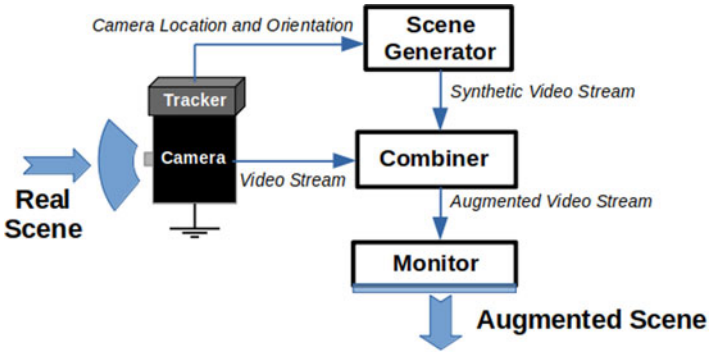

Figure 1. *Monitor-based AR conceptual diagram – adapted from Azuma (1997).*

Thus, an arbitrary vector $\vec{a}$ described with three-dimensional coordinates $\vec{a}_w$ in the *world coordinate system* transforms to the *ship coordinate system* as follows:

$$\vec{a}_s = \begin{bmatrix} x_i & y_i & z_i \\ x_j & y_j & z_j \\ x_k & y_k & z_k \end{bmatrix} \vec{a}_w \tag{2.2}$$

Let $\vec{s}$ be the origin of the ship coordinate system described in the world coordinate system:

$$\vec{s} = s_x\vec{x} + s_y\vec{y} + s_z\vec{z} \tag{2.3}$$

Consider a point P in the environment with coordinates $\vec{p}_w$ in the world coordinate system and $\vec{p}_s$ in the ship coordinate system. The transformation that relates the coordinates of P in each coordinate system can be defined as (Hartley and Zisserman, 2004)

$$\vec{p}_s = \begin{bmatrix} x_i & y_i & z_i & -(x_i s_x + y_i s_y + z_i s_z) \\ x_j & y_j & z_j & -(x_j s_x + y_j s_y + z_j s_z) \\ x_k & y_k & z_k & -(x_k s_x + y_k s_y + z_k s_z) \end{bmatrix} \begin{bmatrix} \vec{p}_w \\ 1 \end{bmatrix} \tag{2.4}$$

$$\vec{p}_w = \begin{bmatrix} x_i & x_j & x_k & s_x \\ y_i & y_j & y_k & s_y \\ z_i & z_j & z_k & s_z \end{bmatrix} \begin{bmatrix} \vec{p}_s \\ 1 \end{bmatrix} \tag{2.5}$$

Further, consider a camera coordinate system described with axes $[\vec{\chi}, \vec{\gamma}, \vec{\kappa}]$. Axis $\vec{\chi}$ is oriented from left to right, axis $\vec{\gamma}$ is oriented downwards and axis $\vec{\kappa}$ is forward oriented. Let each axis from the ship coordinate system be expressed as a combination of axes from the camera coordinate system:

$$\vec{i} = i_\chi\vec{\chi} + i_\gamma\vec{\gamma} + i_\kappa\vec{\kappa}, \quad \vec{j} = j_\chi\vec{\chi} + j_\gamma\vec{\gamma} + j_\kappa\vec{\kappa}, \quad \vec{k} = k_\chi\vec{\chi} + k_\gamma\vec{\gamma} + k_\kappa\vec{\kappa} \tag{2.6}$$

Let $\vec{c}$ be the origin of the camera coordinate system described in the ship coordinate system:

$$\vec{c} = c_i\vec{i} + c_j\vec{j} + c_k\vec{k} \tag{2.7}$$

The transformation relating coordinates of a point P described in the ship coordinate system or in the camera coordinate system may be similarly determined:

$$\vec{p}_c = \begin{bmatrix} i_\chi & j_\chi & k_\chi & -(i_\chi c_i + j_\chi c_j + k_\chi c_k) \\ i_\gamma & j_\gamma & k_\gamma & -(i_\gamma c_i + j_\gamma c_j + k_\gamma c_k) \\ i_\kappa & j_\kappa & k_\kappa & -(i_\kappa c_i + j_\kappa c_j + k_\kappa c_k) \end{bmatrix} \begin{bmatrix} \vec{p}_s \\ 1 \end{bmatrix} \tag{2.8}$$

https://doi.org/10.1017/S0373463321000795 Published online by Cambridge University Press

Figure 2. *Observation of known planar patterns for calibration.*

$$\vec{p}_s = \begin{bmatrix} i_\chi & i_\gamma & i_\kappa & c_i \\ j_\chi & j_\gamma & j_\kappa & c_j \\ k_\chi & k_\gamma & k_\kappa & c_k \end{bmatrix} \begin{bmatrix} \vec{p}_c \\ 1 \end{bmatrix} \tag{2.9}$$

Thus, for a point described with coordinates $\vec{p}_w$ in the world coordinate system, the corresponding coordinates $\vec{p}_c$ in the camera coordinate system can be computed with two sequential transformations. Once a point is described in the camera coordinate system, it is possible to use camera models for its projection as a virtual point in the image scene.

Let $p = [\chi\ \gamma\ \kappa]^{\mathrm{T}}$ be a scene point described in the camera coordinate system and let $i = [u\ v]^{\mathrm{T}}$ be its corresponding image projection *in pixels*. Ideally, the relationship between p and i may be expressed with the *pinhole model*, which is given by (Hartley and Zisserman, 2004)

$$\begin{bmatrix} u \\ v \end{bmatrix} = \begin{bmatrix} f\Delta_u^{-1}\dfrac{\chi}{\kappa} + c_u \\ f\Delta_v^{-1}\dfrac{\gamma}{\kappa} + c_v \end{bmatrix} \tag{2.10}$$

Parameters $[f\Delta_u^{-1}\ \ f\Delta_v^{-1}\ \ c_u\ \ c_v]$ are called *intrinsic parameters* or simply *camera parameters*. This model assumes a process of *central projection*. Light from the scene reaches the camera through a unique point referred to as the *camera centre*. Measurements are sampled in a plane at a distance f from the camera centre. Distance f is usually referred to as the *focal distance* of the camera. The rest of the camera parameters represents the conversion from sensor plane to pixel units. Note that more sophisticated models may be developed by taking into consideration mechanical properties of the lens and typical hardware components (Mahmoudi et al., 2021).

From the correspondences of image coordinates and three-dimensional positions, the camera parameters can be estimated by minimising the error between image observations and their respective model projections. Simplified procedures to estimate the camera parameters are usually based on the camera observation of structures with known dimensions and easily detectable features. A common procedure is based on the observation of a known planar pattern at a few different orientations (Zhang, 2000). Figure 2 shows examples of such calibration patterns as measured by a camera. These planar patterns may be printed with any commercial printer.

The size of each square from the images above is known. Thus, it is possible to define three-dimensional coordinates for each square intersection of the pattern. Calibration parameters may be estimated from these correspondences with open source libraries. The present work uses the open source library *OpenCV* (Bradski, 2000) for most implementations regarding image manipulation. Particularly, the library is used for calibrating the camera, projection of points and synthesis of graphical elements. Figure 3 shows the projection of virtual points associated with the previous calibration pattern using the *OpenCV* library.

Note that all virtual points drawn above belong to a particular plane π coincident with the calibration pattern. An arbitrary plane π may be parametrised by a three-dimensional point π_p belonging to π along with two unitary orthogonal vectors $\pi_{\hat{n}_x}$ and $\pi_{\hat{n}_y}$ parallel to π. Thus, the coordinates of other points p from the plane may be computed from π_p and a linear combination of $\pi_{\hat{n}_x}$ and $\pi_{\hat{n}_y}$:

$$p = \pi_p + \lambda_1\pi_{\hat{n}_x} + \lambda_2\pi_{\hat{n}_y}, \quad \lambda_1, \lambda_2 \in \mathbb{R} \tag{2.11}$$

https://doi.org/10.1017/S0373463321000795 Published online by Cambridge University Press

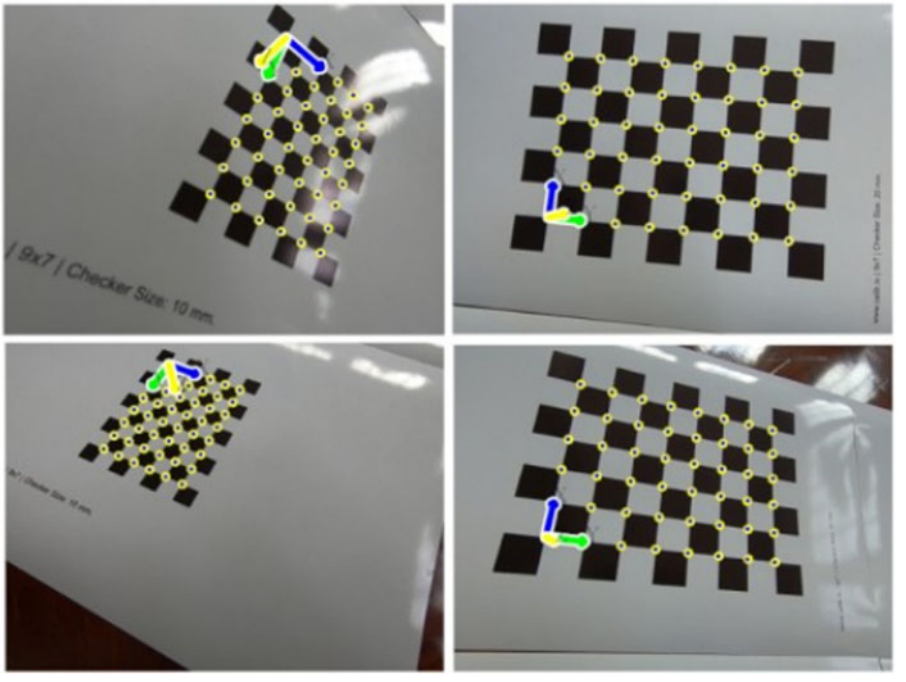

Figure 3. *Detections and corresponding projections of the coplanar virtual points used in the calibration.*

A particular set of points of the plane π may be defined by iterating different pairs (λ_1, λ_2). Assuming that plane parameters π_p, $\pi_{\hat{n}_x}$ and $\pi_{\hat{n}_y}$ are described with respect to the camera coordinate system, auxiliary lines can be straightforwardly projected into the scene with above camera models.

2.3. Experimental setup

Consider a video generated from a navigation experiment by the *TPN-USP Ship Maneuvering Simulation Center*. The TPN-USP is the largest Brazilian ship manoeuvring simulation centre, equipped with three full-mission simulators and three tug stations, as well as one part-task simulator. Tannuri et al. (2014) describe the mathematical model adopted in the simulator, and Makiyama et al. (2020) presents the visualisation framework, able to generate realistic images of the maritime scenario, in real-time. In the video from the experiment, all geometrical parameters are accurately known. Figure 4 illustrates the scene measured by the camera alongside the geometry of the ship from the simulation.

An estimation of the intrinsic parameters of the camera is provided. A set of points with known coordinates may be projected into the image to validate accurateness or to further optimise camera parameters. This is illustrated in Figure 5.

The state of the ship with respect to the world coordinate system is known from the simulation outputs. Figure 6 shows the ship position as a function of time.

Each buoy has fixed coordinates in the world coordinate system during the simulation. Thus, their instantaneous relative position in the ship coordinate system may be computed with expressions from Equations (2.4) and (2.5).

These coordinates in the ship coordinate system may be transformed to the camera coordinate system with expressions from Equations (2.8) and (2.9). Figure 7 shows the instantaneous relative position of one of the buoys with respect to the camera coordinate system.

Further, consider another video from a real experiment of a ship navigating through a channel delimited by nautical buoys with a fixed onboard camera. Figure 8 summarises the installation of

https://doi.org/10.1017/S0373463321000795 Published online by Cambridge University Press

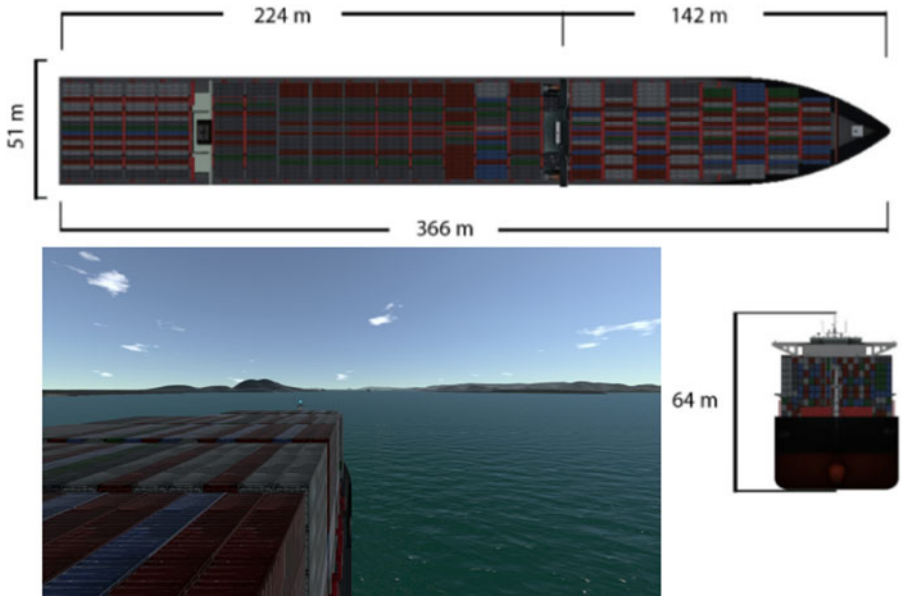

Figure 4. *Ship geometry and visualisation of the simulation experiment.*

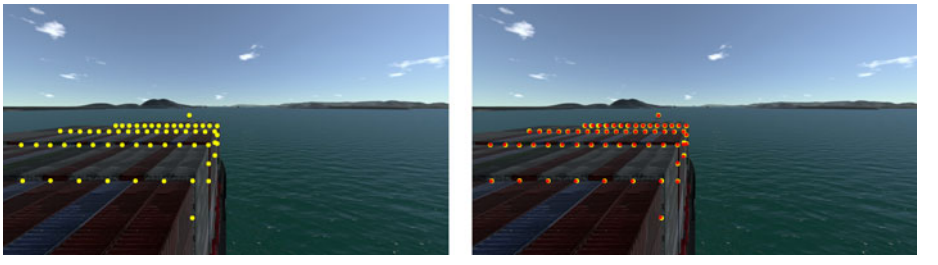

Figure 5. *Detections in the image plane are highlighted on the left; projections from the ship geometry and the camera parameters are shown on the right.*

the camera for this experiment alongside relevant geometrical information from the ship. The ship orientation with respect to the world coordinate system is assumed to be constant and known during the entire experiment. Note that in this real experiment, the instantaneous position of nearby obstacles are unknown.

Intrinsic parameters of the camera are known from calibration procedures, such as the implementation from the *OpenCV* library described in the previous section. The camera position and orientation with respect to the ship frame must be known. Thus, it is interesting to install the camera in a known location from the ship such as in its bridge or its cabin. Then, these parameters may be estimated after installation with information from the ship geometry, which are typically available in the pilot cardboard and the wheelhouse poster, as shown in Figure 8.

If there are known correspondences between camera measurements and three-dimensional coordinates, it is possible to directly estimate the camera position and orientation after installation. For example, consider that all containers from the scene have known dimensions. For each block of adjacent containers, a set of correspondences may be defined with an arbitrary origin and adjacent container points. Then, optimising each set of correspondences yields estimates for the position and orientation for each block of containers. Finally, an estimation for the orientation of the camera may be defined assuming

https://doi.org/10.1017/S0373463321000795 Published online by Cambridge University Press

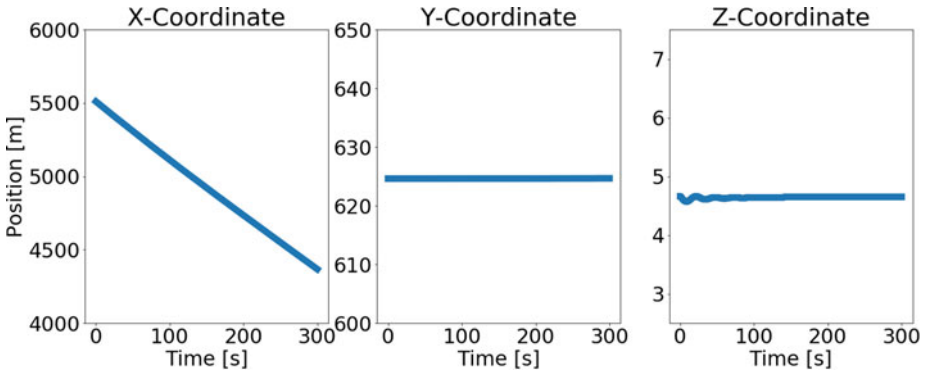

Figure 6. *Ship position as a function of time with respect to the world coordinate system.*

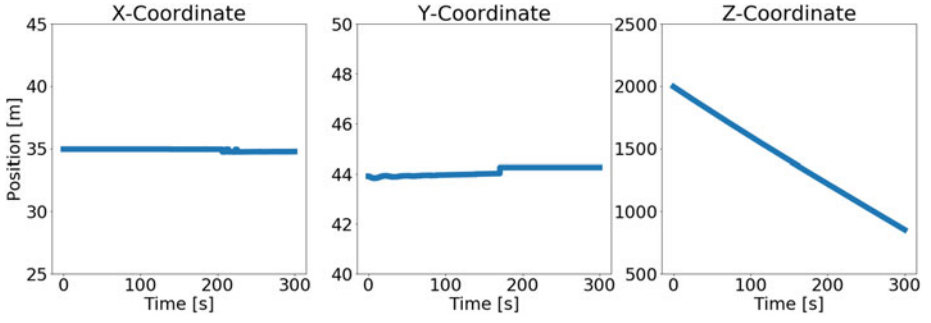

Figure 7. *Buoy position as a function of time with respect to the camera coordinate system.*

the alignment of all containers with the ship coordinate system. Figure 9 exemplifies the procedure with visible points from four blocks of adjacent containers.

Henceforth, the camera position and orientation is assumed to be known with respect to the ship coordinate system. Virtual points around the surface of the sea may be determined from Equation (2.11) by combining the ship draft with the installed camera position and orientation.

For a plane π described with respect to a coordinate system external to the camera, the corresponding plane parameters π_p, $\pi_{\hat{n}_x}$ and $\pi_{\hat{n}_y}$ must be transformed to the camera coordinate system. Assuming knowledge of the rotation matrix relating both frames along with the origin of the external coordinate system, each vector $\pi_{\hat{n}_x}$ and $\pi_{\hat{n}_y}$ may be transformed to the camera coordinate system with a matrix multiplication, as presented in Equation 2.2. The point plane π_p may be transformed similarly as in Equations (2.4), (2.5), (2.8) and (2.9).

3. Results

This section proposes simple virtual information elements that may be rendered on the navigation scene of the previous experiment.

3.1. Simple highlighting

In the simulation experiment, as the position of each buoy in the camera coordinate system is known, it is possible to determine the corresponding projection coordinates in the camera scene by using Equation (2.10). These coordinates may be used for an automatic highlight of such obstacles. A simple form of a highlight is the synthesis of a rectangle as indicated in Figure 10. The obstacle coordinates with respect to the world, ship and camera frame is displayed next to the obstacle projection on the navigation scene.

https://doi.org/10.1017/S0373463321000795 Published online by Cambridge University Press

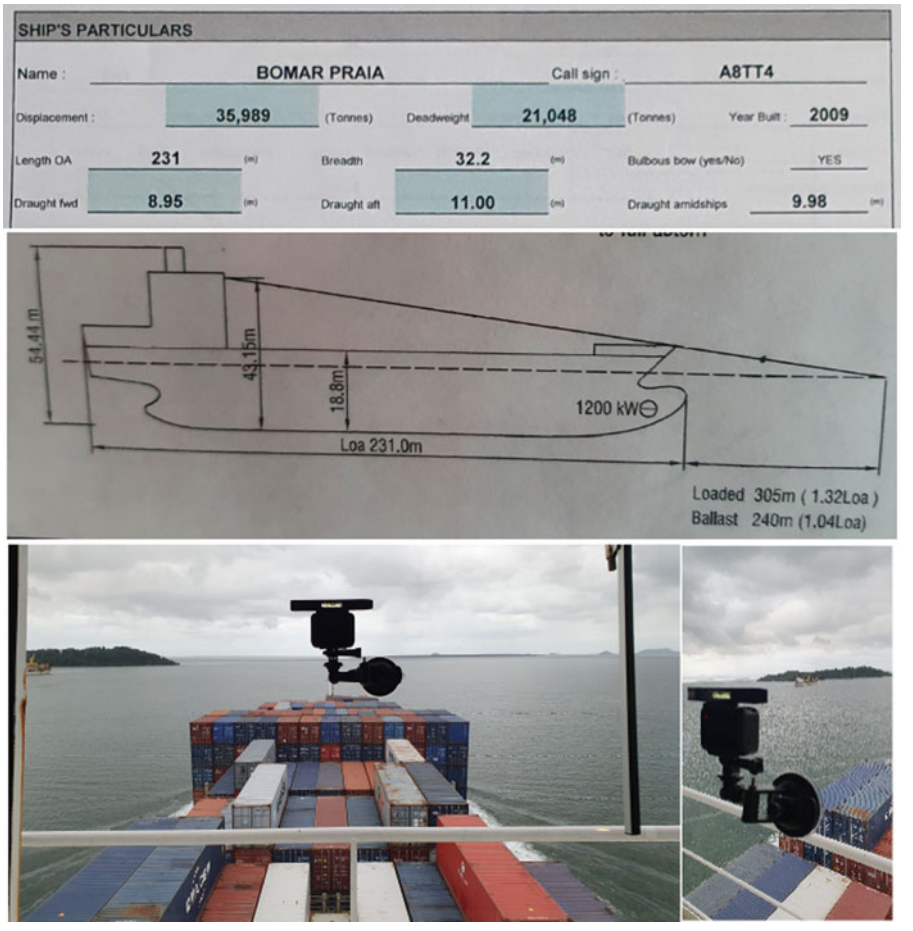

Figure 8. *Geometrical information from the ship (top picture) and installation of the camera in the ship (bottom picture).*

3.2. Planar highlighting

Another form of highlight for a surrounding obstacle may be defined with the projection of a particular set of planar points around its position. Consider the set of points belonging to a plane π according to Equation (2.11). The expression describes a plane π with a point π_p and two unitary vectors $\pi_{\hat{n}_x}$ and $\pi_{\hat{n}_y}$:

$$p = \pi_p + \lambda_1 \pi_{\hat{n}_x} + \lambda_2 \pi_{\hat{n}_y}$$

Assume that unitary vectors $\pi_{\hat{n}_x}$ and $\pi_{\hat{n}_y}$ are aligned with the surface of the sea. Thus, each pair (λ_1, λ_2) yields three-dimensional coordinates of a point near π_p at the surface of the sea. Different highlight visualisations may be determined depending on the set of (λ_1, λ_2).

A *rectangular* highlight consists of two sets of parallel lines in which each line from one set is perpendicular to all lines from the other set. Such a highlight may be defined with the following expressions for pairs (λ_1, λ_2):

$$\begin{bmatrix} \lambda_1 \\ \lambda_2 \end{bmatrix} = \begin{bmatrix} i_x \Delta L_x \\ i_y \Delta L_y \end{bmatrix}, \quad -N_x \leq i_x \leq N_x, \quad -N_y \leq i_y \leq N_y \quad i_x, i_y \in \mathbb{Z} \tag{3.1}$$

where ΔL_x and ΔL_y define the distances between adjacent and parallel lines. The integer i_x iterates from $-N_x$ to N_x and i_y iterates from $-N_y$ to N_y. Adjacent points are connected with lines. Figure 11

https://doi.org/10.1017/S0373463321000795 Published online by Cambridge University Press

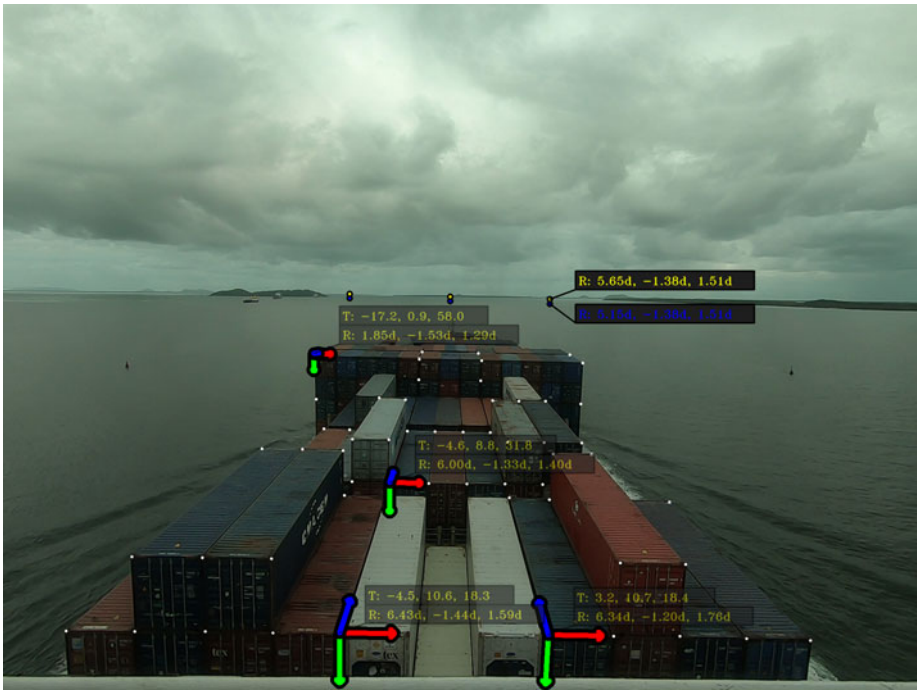

Figure 9. *Camera calibration with visible points from onboard containers.*

Figure 10. *Simple highlighting for each buoy with a summary of coordinates expressed in different frames.*

shows a rectangular highlight computed with the following parameters:

$$\pi_p = \begin{bmatrix} 50 \\ 45 \\ 600 \end{bmatrix}, \quad \pi_{\hat{n}_x} = \begin{bmatrix} 0 \\ 0 \\ 1 \end{bmatrix}, \quad \pi_{\hat{n}_y} = \begin{bmatrix} 1 \\ 0 \\ 0 \end{bmatrix} \tag{3.2}$$

$$\Delta L_x = 40, \quad \Delta L_y = 20, \quad N_x = 10, \quad N_y = 3 \tag{3.3}$$

https://doi.org/10.1017/S0373463321000795 Published online by Cambridge University Press

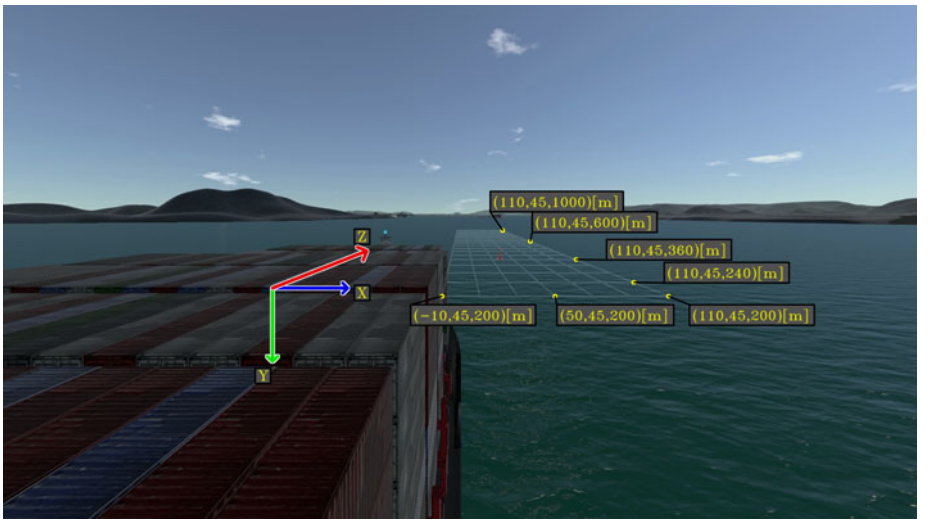

Figure 11. *Auxiliary rectangular grid for points in the camera frame. Each rectangle of the grid has dimensions* 40 $m \times 20$ m.

Alternatively, a *circular* highlight consists of sets of co-planar circles around a given point π_p. Each point from each circle may be described by an angle θ with respect to the plane vector $\pi_{\hat{n}_x}$ and by a radius r_i with respect to the plane point π_p. Such a highlight may be defined by the following expressions for pairs (λ_1, λ_2):

$$\begin{bmatrix}\lambda_1\\ \lambda_2\end{bmatrix} = \begin{bmatrix}r_i\cos(\theta)\\ r_i\sin(\theta)\end{bmatrix} \Rightarrow \begin{cases}\theta \text{ variable and } r_i \text{ fixed:} & \Theta_{\min} \le \theta \le \Theta_{\max}, \quad r_i \in R_r\\ r_i \text{ variable and } \theta \text{ fixed:} & 0 \le r_i \le \max(R_r), \quad \theta \in \Theta_r\end{cases} \tag{3.4}$$

where R_r is a list with different radius to be displayed, $\max(R_r)$ represents the element of maximum value in R_r and r_i denotes an element of R_r that is being iterated. Pairs (λ_1, λ_2) generated by the variation of θ with a fixed r_i yields circles with radius r_i. These circles may be divided into sections by the computation of (λ_1, λ_2) with a fixed θ and variable r_i. Here Θ_r is a list with different θ for sectioning such circles. Figure 12 shows a circular highlight computed with the following parameters:

$$\pi_p = \begin{bmatrix}60\\ 45\\ 200\end{bmatrix}, \quad \pi_{\hat{n}_x} = \begin{bmatrix}0\\ 0\\ 1\end{bmatrix}, \quad \pi_{\hat{n}_y} = \begin{bmatrix}1\\ 0\\ 0\end{bmatrix} \tag{3.5}$$

$$R_r = [50{\cdot}0, 300{\cdot}0, 1800{\cdot}0], \quad -\pi \le \theta \le \pi, \quad \Theta_r = \left[0, \frac{\pi}{16}, \ldots, n\frac{\pi}{16}\right] \quad n \in \mathbb{Z} \tag{3.6}$$

If there are external systems providing information about surrounding obstacles at sea, such as their relative position with respect to the ship, their projection in the camera scene may be automatically enhanced by virtual elements to assist in their identification. This situation is exemplified by the video from the experiment of the ship manoeuvring simulator. Generally, for a real implementation of such an automatic highlight, it is necessary to integrate the system with typical onboard equipment from the ship. In the video from the real experiment, where no prior information about surrounding obstacles is available, image-processing techniques may be also applied to determine the projection of each obstacle in the navigation scene.

Furthermore, note that the aforementioned auxiliary lines defined by Equations (2.11), (3.1) and (3.4) may be used to assist in the spatial perception of the scene. A potentially useful application would be to highlight the expected route in the navigation scene to assist in its perception by operators. Instead of rendering a planar highlight around the coordinates of a given obstacle, a planar highlight around points from the expected trajectory may assist in the perception of the ship route.

https://doi.org/10.1017/S0373463321000795 Published online by Cambridge University Press

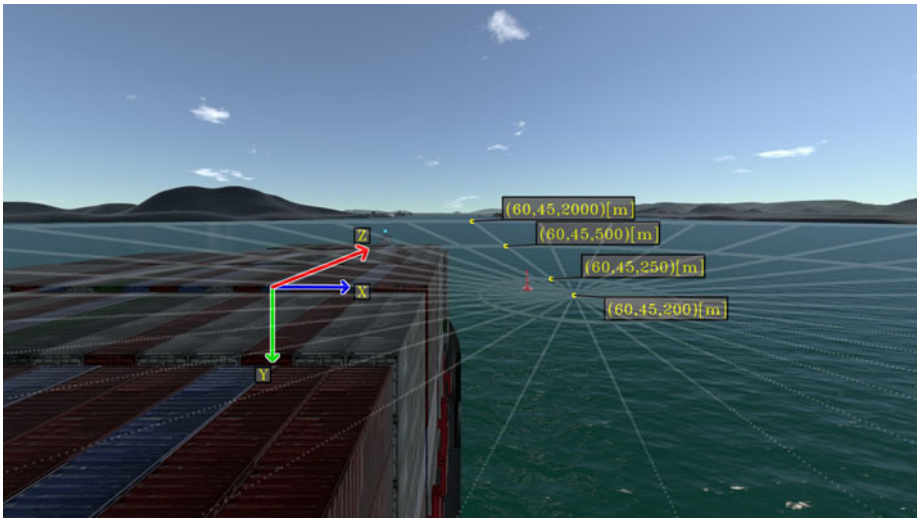

Figure 12. *Auxiliary cylindrical grid for points in the camera frame. Each circle is divided into 32 sections.*

Figure 13. *Rectangular highlight showing the expected trajectory for the ship in the simulation.*

4. Discussion

In this section, potential applications of navigational assistance in restricted waters are discussed in terms of the proposed visual elements.

4.1. Route highlighting

In the previous simulation, the ship is navigating in a straight line with known velocity. In such situations, a rectangular highlight in front of the ship corresponds to the expected trajectory of the ship. Figure 13 exemplifies the implementation in the previous simulation experiment with a rectangular highlight delimiting the expected trajectory of the ship.

https://doi.org/10.1017/S0373463321000795 Published online by Cambridge University Press

Figure 14. *Rectangular highlight showing expected trajectory for the ship in reality.*

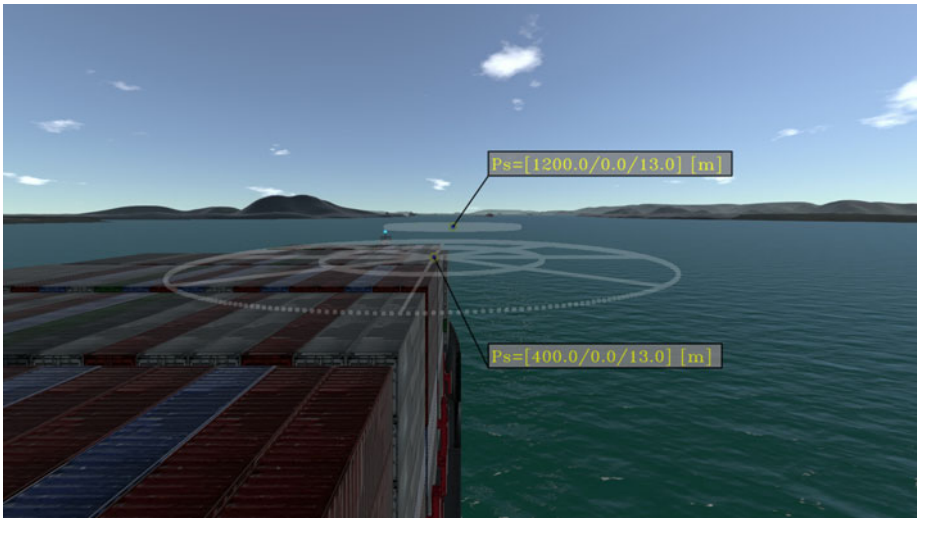

Figure 15. *Circular highlight representing waypoints of the expected trajectory for the ship in the simulation.*

A similar rectangular highlight may be drawn on top of the video from the real experiment as the ship navigates with approximately constant velocity in a straight line. Figure 14 illustrates this implementation.

Another useful representation for the expected trajectory of the ship is in the form of waypoints. Each waypoint may be projected into the image scene with a circular highlight. As the ship is travelling with constant velocity, its trajectory may be represented by colinear waypoints. Figure 15 illustrates the visualisation with two waypoints in front of the ship.

https://doi.org/10.1017/S0373463321000795 Published online by Cambridge University Press

Figure 16. *Circular highlight representing waypoints of the expected trajectory for the ship in reality.*

Figure 17. *Information highlight for each buoy in the simulation.*

Figure 16 illustrates a similar implementation in the recorded video from the aforementioned real experiment.

4.2. Obstacle highlighting

Let each buoy of the previous simulation be an obstacle to be highlighted in the image scene with a *simple highlight*. Assume that information about surrounding obstacles is available and consider an additional onboard system that is able to provide information about nearby obstacles in the form of different

https://doi.org/10.1017/S0373463321000795 Published online by Cambridge University Press

attributes. For example, attributes such as identification, name, type, status, position with respect to map and position with respect to ship. Further, assume that the corresponding obstacle attributes are automatically rendered into a graphical summary. Such a graphical summary may be overlaid next to the obstacle projection in the navigation scene, as shown in Figure 17.

Note that points that are very far from the ship have a corresponding small projection in the image scene. It is interesting to estimate the maximum distance in which an obstacle is still observable by the camera. A simplified analysis may be carried out as follows. Consider a *pinhole* model expressed by the set of intrinsic parameters $[f_u, f_v, c_u, c_v]$. Further, assume that the obstacle is represented as a simple planar square object with size L positioned at a point p. Each vertex p^{li} of this square may be projected into the image scene:

$$
\begin{aligned}
p = \begin{bmatrix} p_\chi \\ p_\gamma \\ p_\kappa \end{bmatrix} \Rightarrow \begin{bmatrix} u \\ v \end{bmatrix} &= \begin{bmatrix} f\Delta_u^{-1}\dfrac{p_\chi}{p_\kappa} + c_u \\ f\Delta_v^{-1}\dfrac{p_\gamma}{p_\kappa} + c_v \end{bmatrix} \\
p^{l1} = p + \frac{L}{2}\begin{bmatrix} 1 \\ 1 \\ 0 \end{bmatrix} = \begin{bmatrix} p_\chi + 0{\cdot}5L \\ p_\gamma + 0{\cdot}5L \\ p_\kappa \end{bmatrix} \Rightarrow \begin{bmatrix} u^{l1} \\ v^{l1} \end{bmatrix} &= \begin{bmatrix} f\Delta_u^{-1}\dfrac{p_\chi + 0{\cdot}5L}{p_\kappa} + c_u \\ f\Delta_v^{-1}\dfrac{p_\gamma + 0{\cdot}5L}{p_\kappa} + c_v \end{bmatrix} \\
p^{l2} = p + \frac{L}{2}\begin{bmatrix} 1 \\ -1 \\ 0 \end{bmatrix} = \begin{bmatrix} p_\chi + 0{\cdot}5L \\ p_\gamma - 0{\cdot}5L \\ p_\kappa \end{bmatrix} \Rightarrow \begin{bmatrix} u^{l2} \\ v^{l2} \end{bmatrix} &= \begin{bmatrix} f\Delta_u^{-1}\dfrac{p_\chi + 0{\cdot}5L}{p_\kappa} + c_u \\ f\Delta_v^{-1}\dfrac{p_\gamma - 0{\cdot}5L}{p_\kappa} + c_v \end{bmatrix} \\
p^{l3} = p + \frac{L}{2}\begin{bmatrix} -1 \\ -1 \\ 0 \end{bmatrix} = \begin{bmatrix} p_\chi - 0{\cdot}5L \\ p_\gamma - 0{\cdot}5L \\ p_\kappa \end{bmatrix} \Rightarrow \begin{bmatrix} u^{l3} \\ v^{l3} \end{bmatrix} &= \begin{bmatrix} f\Delta_u^{-1}\dfrac{p_\chi - 0{\cdot}5L}{p_\kappa} + c_u \\ f\Delta_v^{-1}\dfrac{p_\gamma - 0{\cdot}5L}{p_\kappa} + c_v \end{bmatrix} \\
p^{l4} = p + \frac{L}{2}\begin{bmatrix} -1 \\ 1 \\ 0 \end{bmatrix} = \begin{bmatrix} p_\chi - 0{\cdot}5L \\ p_\gamma + 0{\cdot}5L \\ p_\kappa \end{bmatrix} \Rightarrow \begin{bmatrix} u^{l4} \\ v^{l4} \end{bmatrix} &= \begin{bmatrix} f\Delta_u^{-1}\dfrac{p_\chi - 0{\cdot}5L}{p_\kappa} + c_u \\ f\Delta_v^{-1}\dfrac{p_\gamma + 0{\cdot}5L}{p_\kappa} + c_v \end{bmatrix}
\end{aligned}
\tag{4.1}
$$

The projection area a_p in pixel^2 may be computed as a function of the projection of each vertex of the square:

$$
\begin{aligned}
\begin{bmatrix} u_M^l \\ v_M^l \end{bmatrix} = \sum_{i=1}^{4} \frac{1}{4}\begin{bmatrix} u^{li} \\ v^{li} \end{bmatrix} \Rightarrow \begin{bmatrix} u_c^{li} \\ v_c^{li} \end{bmatrix} &= \begin{bmatrix} u^{li} - u_M^l \\ v^{li} - v_M^l \end{bmatrix} \\
a_p = \frac{1}{2}(\|u_c^{l1}v_c^{l2} + u_c^{l2}v_c^{l3} + u_c^{l3}v_c^{l4} + u_c^{l4}v_c^{l1} - u_c^{l2}v_c^{l1} - u_c^{l3}v_c^{l2} - u_c^{l4}v_c^{l3} - u_c^{l1}v_c^{l4}\|)
\end{aligned}
\tag{4.2}
$$

Visible objects should have a projection area a_p bigger than 1 pixel^2. Table 1 presents a_p as a function of different L at points $p_1 = [50, 15, 200]$, $p_2 = [50, 15, 2{,}000]$ and $p_3 = [50, 15, 10{,}000]$ for intrinsic camera parameters $[f_u, f_v, c_u, c_v] = [790, 770, 960, 440]$.

Thus, for example, a square with an area of 1 m^2 would not be visible at a distance of 2,000 m but would be detectable at a distance of 200 m from the camera. Still, if a_p is not sufficiently greater than 1 px^2, its projection in the image scene may be very difficult to acknowledge. In such scenarios, the scene could be *zoomed-in* around the obstacle projection to assist in their identification. The open source library *OpenCV* (Bradski, 2000) provides *zoom-in* operations that may be used for rendering

https://doi.org/10.1017/S0373463321000795 Published online by Cambridge University Press

Table 1. *Calculated a_p at p_i^W for different values of L.*

L (m)	a_p at p_1 (px^2)	a_p at p_2 (px^2)	a_p at p_3 (px^2)
1	15·306	0·153	0·006
5	382·656	3·827	0·153
10	1530·625	15·306	0·612
20	6122·500	61·225	2·449
50	38265·625	382·656	15·306

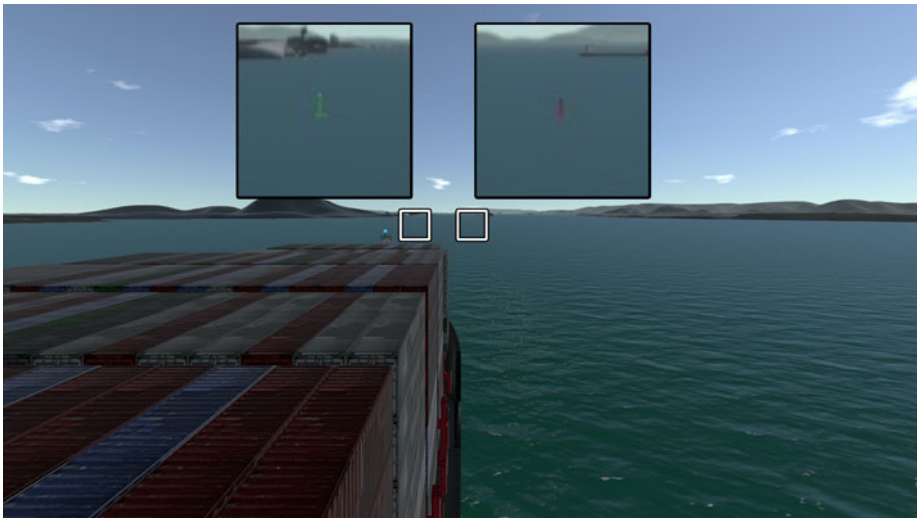

Figure 18. *Amplified windows of surrounding obstacle projections in the simulation.*

such amplifications of far obstacles. These amplified windows may be automatically displayed next to each obstacle projection as illustrated in Figure 18.

Figure 19 shows two amplified windows for each buoy of the aforementioned real experiment. Different from the simulation experiment, the relative position of these buoys with respect to the ship and the camera are not known. In such cases, each zoom window needs to be manually initialised by an operator. Note that image processing methods may be performed for further automatic tracking of each initialised region.

4.3. Spatial perception

In cases where external information about surrounding obstacles is not available, it is possible to estimate the relative position of visible obstacles in the image scene with planar highlights. Figure 20 shows a rectangular highlight with points described in the ship coordinate system. An estimation for the relative position of the buoy may be inferred by the intersection of the buoy projection in the image scene with each auxiliary line of the rectangular grid.

Figure 21 shows a rectangular highlight in the real experiments with a grid of dimensions 100 m × 25 m.

Note that the right buoy intersects the rectangular grid at the sixth parallel line of the grid, which represents an approximate lateral distance of $25 \times 6 = 150$ m. Correspondingly, the left buoy intersects the rectangular grid at the fifth parallel line of the grid, which yields an approximate lateral distance of $25 \times 5 = 125$ m. Combining both results yields estimates of 275 m for the distance between both buoys.

https://doi.org/10.1017/S0373463321000795 Published online by Cambridge University Press

Figure 19. *Amplified windows of surrounding obstacle projections in reality.*

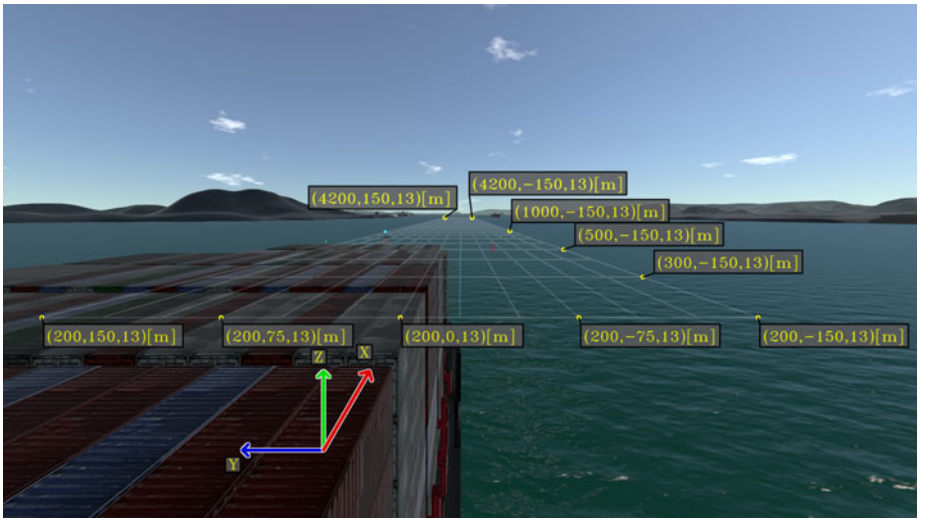

Figure 20. *Auxiliary rectangular grid for estimating the relative position of surrounding obstacles in the simulation. Each rectangle of the grid has dimensions* 100 $m \times 25$ *m.*

Accordingly, the theoretical distance between them is approximately 280 m when both buoys are in their map position.

Another useful representation for estimating the relative position of the buoy may be displayed with a circular highlight. Figure 22 shows a circular highlight with points described in the ship coordinate system.

Similarly, an estimation for the buoy relative position may be determined from the intersection of its projection with each auxiliary line. From the augmented scene of the above example, it is possible to

https://doi.org/10.1017/S0373463321000795 Published online by Cambridge University Press

Figure 21. *Auxiliary rectangular grid for estimating the relative position of surrounding obstacles in reality. Each rectangle of the grid has dimensions* $100\ m \times 25\ m$.

estimate that the buoy is at an approximate distance of 500 m from the ship with an angle of $-9°$ with respect to the ship x-axis.

Note that the augmented scenes from this section are designed considering a scenario of a ship travelling in restricted waters with fixed obstacles. In such scenarios, to prevent collisions, it is important that operators acknowledge the relative position of surrounding obstacles along the expected trajectory of the ship. As the proposed enhanced scenes from this section assist in the perception of these important elements, these scenes may be combined into a navigational assistance equipment based on augmented reality.

Alternative enhanced scenes may be adapted from the current work towards other navigation scenarios. As the development of optimal visualisations combining pertinent virtual elements depends on the particular operation of the user, further research is suggested to cover other types of standardised navigation operations.

5. Conclusion

Foundations regarding augmented reality methods were discussed throughout the paper. Examples of enhanced scenes for a monitor AR solution were proposed in the context of a ship navigating with constant velocity in restricted waters. As each augmented scene assist in the perception of the navigation environment, these visualisations are potentially helpful for the corresponding ship operators. However, to adequately embed these augmented scenes into helpful equipment, designed visualisations shall be further validated considering usability requirements from typical operations.

The development of an operational augmented reality system for navigational assistance is still a complex task. For a real implementation, the ship state with respect to the world coordinate system needs to be accurately determined along with the camera parameters. To ensure a proper alignment between real and virtual marks, information regarding the truth position of nearby obstacles and ship

https://doi.org/10.1017/S0373463321000795 Published online by Cambridge University Press

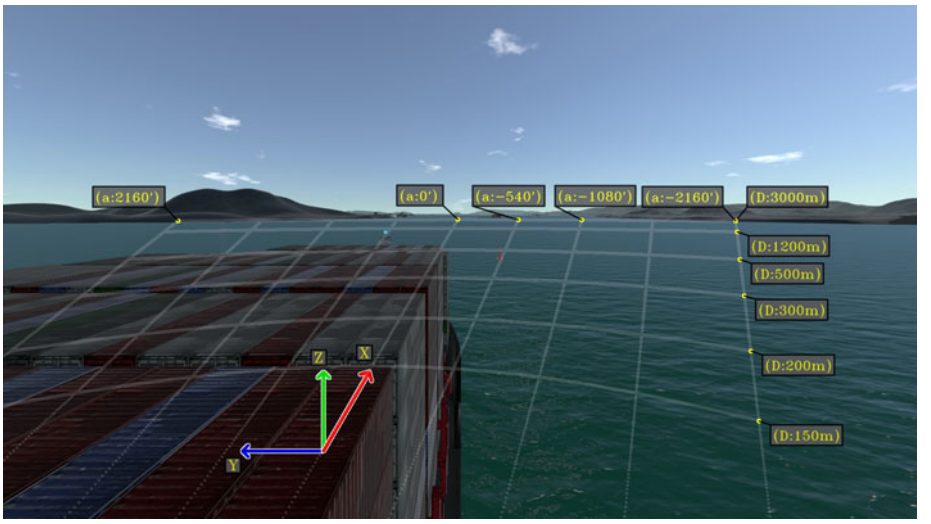

Figure 22. *Auxiliary lines described with respect to the ship frame. Lines are drawn ranging from* $\theta_{min} = -36° = -2{,}160'$ *to* $\theta_{max} = 36° = 2{,}160'$.

surroundings needs to be accurately determined by onboard ship systems. Additionally, the integration of such different equipment needs to robustly address real-time constraints which may be inherently complex.

Despite the challenges, the development of equipment with augmented reality methods is further suggested as it has the potential to significantly contribute to the overall efficiency and safety of maritime operations. It should be noted that although further research with real implementations may be extremely expensive owing to the requirement of high-precision sensors, usability research may be appropriately performed with any full-mission ship manoeuvring simulator as presented in the present work. Therefore, as a general recommendation, the authors suggest that user interface research for MAR systems should be preliminary performed with a ship manoeuvring simulator. In such simulations, all geometrical parameters are known, which facilitates the development of ideal visualisations without the need of extremely accurate equipment.

Acknowledgements. The authors thank Petrobras and Brazilian National Agency for Petroleum, Natural Gas and Biofuels (ANP) for supporting this research project. B.G.L. thanks the Coordination for the Improvement of Higher Education Personnel (CAPES) for the scholarship. E.A.T. thanks the CNPq – Brazilian National Council for Scientific and Technological Development for the research grant (process 310127/2020-3).

References

Azuma, R. T. (1997). A survey of augmented reality. *Presence: Teleoperators & Virtual Environments*, **6**(4), 355–385.

Bradski, G. (2000). The OpenCV library. *Dr Dobb's J. Software Tools*, **25**, 120–125.

Hareide, O. and Ostnes, R. (2017). Maritime usability study by analysing eye tracking data. *Journal of Navigation*, **70**(5), 927–943. doi:10.1017/S0373463317000182

Hartley, R. and Zisserman, A. (2004). *Multiple View Geometry in Computer Vision*. 2nd ed. Cambridge: Cambridge University Press.

Holder, E. and Pecota, S. (2011). Maritime head-up display: a preliminary evaluation. *Journal of Navigation*, **64**(4), 573–594. doi:10.1017/S0373463311000191

Hong, T. C., Andrew, H. S. Y. and Kenny, C. W. L. (2015). Assessing the situation awareness of operators using maritime augmented reality system (MARS). *Proceedings of the Human Factors and Ergonomics Society Annual Meeting*, **59**(1), 1722–1726. doi:10.1177/1541931215591372

Kopacz, Z., Morgaś, W. and Urbański, J. (2001). The maritime safety system, its main components and elements. *Journal of Navigation*, **54**(2), 199–211. doi:10.1017/S0373463301001205

Kopacz, Z., Morgaś, W. and Urbański, J. (2004). The changes in maritime navigation and the competences of navigators. *Journal of Navigation*, **57**(1), 73–83. doi:10.1017/S0373463303002522

Laera, F., Fiorentino, M., Evangelista, A., Boccaccio, A., Manghisi, V., Gabbard, J. and Foglia, M. (2021). Augmented reality for maritime navigation data visualisation: a systematic review, issues and perspectives. *Journal of Navigation*, **74**(5), 1073–1090. doi:10.1017/S0373463321000412

Maglić, L. and Zec, D. (2020). The impact of bridge alerts on navigating officers. *Journal of Navigation*, **73**(2), 421–432. doi:10.1017/S0373463319000687

Mahmoudi, A., Sabzehparvar, M. and Mortazavi, M. (2021). A virtual environment for evaluation of computer vision algorithms under general airborne camera imperfections. *Journal of Navigation*, **74**(4), 801–821. doi:10.1017/S0373463321000060

Makiyama, H. S., Szilagyi, E., Pereira, G. H., Alves, L. R. R., Kodama, B. M., Taniguchi, D. and Tannuri, E. A. (2020). Computational Graphics and Immersive Technologies Applied to a Ship Maneuvering Simulator. *19th International Conference on Geometry and Graphics - ICGG, Sao Paulo, Brazil, 2020, 2021*, 626–635.

Mihoc, A. and Cater, K. (2017). Augmenting Navigational Aids: The Development of an Assistive Maritime Navigation Application. In *World Academy of Science, Engineering and Technology, International Science Index, Computer and Information Engineering*. 1st ed., Vol. 3, pp. 2432. ICVAR 2017 : 19th International Conference on Virtual and Augmented Reality, Singapore, Singapore, 8/01/17. https://doi.org/10.1999/1307-6892/10007671. https://research-information.bris.ac.uk/en/publications/augmenting-navigationalaids- the-development-of-an-assistive-mari

Milgram, P., Takemura, H., Utsumi, A., Kishino, F. (1995). Augmented Reality: A Class of Displays on the Reality-Virtuality Continuum. In *Proc. SPIE 2351, Telemanipulator and Telepresence Technologies*, *Boston, MA, United States,* pp. 282–292. doi: 10.1117/12.197321.

Morgère, J., Diguet, J. and Laurent, J. (2014). Electronic Navigational Chart Generator for a Marine Mobile Augmented Reality System. *2014 Oceans - St. John's, 2014*, 1–9. Available at https://doi.org/10.1109/OCEANS.2014.7003021.

Oh, J., Park, S. and Kwon, O.-S. (2016). Advanced navigation aids system based on augmented reality. *International Journal of e-Navigation and Maritime Economy*, **5**, 21–31.

Sanchez-Gonzalez, P. L., Díaz-Gutiérrez, D., Leo, T. J. and Núñez-Rivas, L. R. (2019). Toward digitalization of maritime transport? *Sensors*, **19**(4), 926. doi:10.3390/s19040926

Sutherland, I. E. (1968). A Head-Mounted Three-Dimensional Display. In *Proceedings of the December 9–11, 1968, Fall Joint Computer Conference, Part I*, *San Francisco, CA, United States, 1968,* 757–764.

Tannuri, E. A., Rateiro, F., Fucatu, C. H., Ferreira, M. D., Masetti, I. Q. and Nishimoto, K. (2014). Modular Mathematical Model for a Low-Speed Maneuvering Simulator. *Proceedings of the ASME 2014 33rd International Conference on Ocean, Offshore and Arctic Engineering. Volume 1B: Offshore Technology. San Francisco, California, USA, 2014.* V01BT01A036. ASME. https://doi.org/10.1115/OMAE2014-24414.

Zhang, Z. (2000). A flexible new technique for camera calibration. *IEEE Transactions on Pattern Analysis and Machine Intelligence*, **22**(11), 1330–1334.

Cite this article: Leite BG, Sinohara HT, Maruyama N, Tannuri EA (2022). Maritime navigational assistance by visual augmentation. *The Journal of Navigation* **75**: 1, 57–75. https://doi.org/10.1017/S0373463321000795